MELT-BLENDED TERNARY POLYMER-CLAY COMPOSITES FOR ADDITIVE MANUFACTURING

Ryan P. Mann[a,b,*], Larry E. Luster[a,b], and Michael J. Bortner[a,b,**]

[a] Department of Chemical Engineering, Virginia Polytechnic Institute and State University, Blacksburg, VA

[b] Macromolecules Innovation Institute, Virginia Polytechnic Institute and State University, Blacksburg, VA

Abstract

Current direct air-based contaminant capture techniques make use of packed beds with adsorbents of simple geometries; however, these mechanisms suffer from high pressure drop, particle attrition, and a failure to maximize exposed surface area. By creating novel composites with high surface area geometries, we aim to improve current packed bed methods for carbon capture. We have developed a novel 3D printable polymer/clay composite of Poly(lactic acid) (PLA), bentonite, and zeolite to be used for contaminant removal applications. Parts manufactured with unique geometries through fused-filament-fabrication can then be post-processed through Shaping, Debinding, and Sintering (SDS) to maximize the surface area ratio available for contaminant capture. We perform thermo-mechanical analysis to assess the stiffness and suitability of our clay composite for SDS. We utilize microscopy and mechanical testing of the printed parts to analyze the clay dispersion and exfoliation levels of our composites. Based on the outcome of the testing we iteratively adjust composition and/or process parameters until successful morphology is realized. We explore the clay loading level and exfoliation threshold required for successful SDS to be performed with our composite system via additive manufacturing.

Introduction

Air-based contaminant capture systems play a key role in establishing breathable environments in difficult atmospheres such as on the International Space Station (ISS). However, current methods rely on a series of packed beds with zeolites to remove target adsorbents (primarily CO_2), which suffer from a number of drawbacks, including high pressure drop, particle attrition, and a failure to maximize exposed surface area. [(1)(2)]

Zeolites, like those used on the ISS, are unique clay molecules that can adsorb molecules at both the physical and chemical level.[(3)] Zeolites inherently possess a structure composed of micro and meso pores. While each species of zeolite has a different pore structure, they all possess pores that have been observed to act as cages.[(4)] In particular, zeolite's unique intramolecular cage structure (formed from its alumina-silica network) has been noticed to capture gaseous particles, including CO_2 gas.[(5)]

Bentonite is another material of interest for direct air capture as a clay compound with a similar molecular structure as zeolite. However, it takes the shape of flat platelets instead of zeolite's cage-structure. It has been used in direct ink writing (DIW) as a plasticizer in compounds to lower the viscosity of the composite.[(6)] We hypothesize that this should help with dispersion. Both zeolite and bentonite undergo ambient contaminant (atmospheric moisture and/or solvent that has been evaporated from samples in the same containment unit) degradation when heated between 400°C-650°C, while zeolite has been observed to experience minor adsorption/desorption of ambient gasses at temperatures greater than 650°C.[(5)]

Additive manufacturing allows for complex shaping that takes advantage of the inherent pore structure of zeolites. Zeolite compounds have previously been 3D printed in other polymer composites, primarily using (DIW).[(7)(8)(9)] Fused filament fabrication (FFF) is another way to 3D print materials, and one advantage it holds over DIW is its ability to control finer details of a small print. This is particularly important when printing monolith structures, where the pore size/placement must be very precise in order to be effective.[(5)(7)] A polymer feedstock is required as a matrix to shape desired filler particles through FFF. One such feedstock is poly(lactic acid) (PLA) is an amorphous compound that is commonly used as filament in additive manufacturing due to its low cost, high availability, and practicability to print and degrade.[(10)] Additionally, PLA-zeolite composite filaments produced through FFF have also been shown to adsorb ammonia in aqueous environments.[(11)]

Shaping, debinding, and sintering (SDS) is a set of processing conditions to help produce printed structures with the intended shape and composition. In the shaping step, the filament (composed of binders and additives) is printed into the desired shape. In the debinding step, the main binder is removed from the structure, usually either via thermal degradation or solvent extraction. There can be multiple debinding steps depending on the number of binders that are desired to be removed.[12] Sintering involves densification of the remaining ceramic (typically at 2/3 to 3/4 of the ceramic's melting temperature) by creating and then growing grain boundaries, followed by closing the gaps formed during the debinding step. In the event zeolite and bentonite particles are not able to bond and form grain boundaries, sintering will be unsuccessful, and the result will be a ceramic powder mixture. Therefore, dispersion of both clays and the exfoliation of bentonite platelets are required for successful sintering. SDS allows for all the benefits of additive manufacturing (including ease of use and availability) while also allowing the user to precisely control the composition and pore structure of the final structure.

To probe our level of exfoliation, we must account for the particle-particle and particle-polymer interactions in our system. Traditionally, we could predict our particle exfoliation using the hard sphere model, in which all components are assumed to be non-interacting with a hard core.[13] However, this model fails to account for specific interactions, permeable volumes, or differences in aspect ratio/geometry, all of which are present in real systems.[14] For our complex clay-polymer system, interparticle and particle-polymer interactions are key, which are unaccounted for in the hard sphere model. For example, while PLA (among other polymers) may be a hard sphere at its base, its chains can flow and interact with the bentonite platelets. Additionally, if a certain activation energy is overcome in a collision, the bentonite agglomerates can break into their base platelets. Since bentonite and zeolite are charged particles, there are bonding forces greater than those of Van der Waals forces present, another item not considered in the hard sphere model (Figure 2).

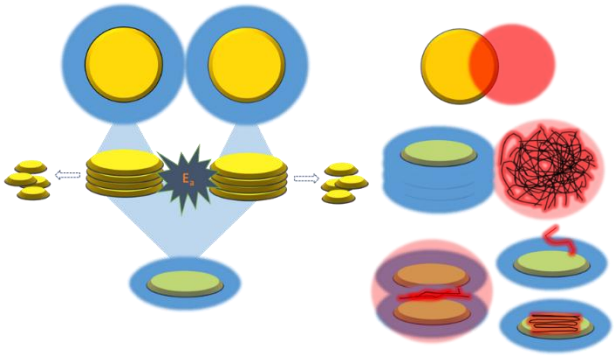

Figure 1. Interactions inherent to the clay-polymer system don't obey the hard sphere model. These include the activation energy to break bentonite platelets and the movement of polymer chains within the free volume of the system.

A hierarchical pore structure is important for capturing gas particles using zeolite, including the meso and micro pores inherent in the zeolite as well as macropores between molecules.[8] In order to maximize CO_2 capture from a monolith structure, we desire a compound that has a hierarchical pore structure, which can be produced using SDS. By introducing bentonite as a structural additive to encourage sintering among zeolite particles, we aim to produce a filament that can be processed by FFF and SDS to produce high surface geometries. To improve upon current packed bed adsorption technologies, these printed parts must weigh less and take up less space while maintaining CO_2 adsorption capabilities. Specific to the SDS steps in our polymer, PLA will act as the semi-permanent binder, while bentonite acts as a permanent binder along with the zeolite as an additive (Figure 2).

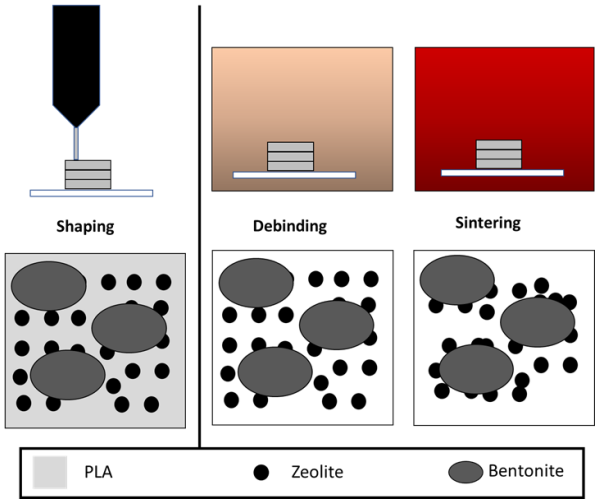

Figure 2. Shaping-debinding-sintering of the PLA-zeolite-bentonite system involves forming the desired structure from a filament with all three components, followed by burning off the PLA resin, and finally sintering the remaining bentonite and zeolite particles to form a network that will undergo densification.

In order to characterize the filament composition feasibility for SDS, multiple thermal and mechanical tests must be performed on both the individual components and the compounded filament. Our work explores the characterization of zeolite, bentonite, and PLA, as well as examining the structure-process-property relationships in a novel, 3D-printable PLA-clay composite. We present novel composites with high surface area geometries that aim to improve on current packed bed methods for carbon capture.

Experimental Section

Materials

Zeolite (molecular sieves, 13x powder, 2µm avg. size, $Na_{86}[(AlO_2)_{86}(SiO_2)_{106}]$ ·H2O) was purchased from Sigma-Aldrich. Neat PLA pellets were purchased from 3DXTech. Bentonite ($Al_2H_2O_6Si$) was purchased from Sigma Aldrich.

Filament Compounding

Filaments that were desired to be 80% PLA, 10% zeolite, and 10% bentonite by weight were compounded via two methods:

Single screw extrusion used a Killion Model KL-100 with a 3.5 mm die and 25mm screw diameter. Powders were dried in a vacuum oven for at least 72 hours and then mixed with the PLA pellets until pellets were coated. The resulting powder/pellet mixture was put through the hopper and extruded with a temperature profile from throat to die of: 160 - 165-165-170-155 °C. The extrudate was cooled by convective air cooling by an Airpath and wound to a desired diameter of 1.75±0.05mm. Filaments that were pelletized (Filabot Pelletizer) and extruded for a second time (with no additional material) were first dried for at least 48 hours before extrusion under the same conditions outlined above.

Twin screw extrusion used a process adapted from Kennedy et al. to mix the powders and pellets during extrusion in a ThermoFisher Process 11 with a 2 mm die and 11mm screw diameter.[11] Powders were mixed by hand in equal weight proportions and dried for 8 hours before extrusion. The PLA was added through one hopper using a 11 mm single-screw feeder, and the zeolite/bentonite mixture was added through a second hopper using a volumetric MiniTwin feeder. Nominal mass concentrations for the feeding zones were characterized using the method from Kennedy et al., where flow rates were calculated by developing separate standard curves for the PLA pellets and zeolite to achieve the desired 20 wt.% clay by weighing the material mass delivered after 60 s.[14] The temperature profile from throat to die was 178-185-185-200-210-210-195-156 °C. The filament was cooled by convective air cooling by an Airpath and wound to a desired diameter of 1.75±0.05mm.

Thermo-Gravimetric Analysis (TGA)

A TA Instruments TGA5500 was used to analyze material degradation characteristics. Samples weighing between 3-5mg were tested at a ramp rate of 5°C/min from 30°C to 800°C. Samples were dried for at least 24 hours prior to testing.

Differential Scanning Calorimetry (DSC)

A TA Instruments DSC2500 was used to test samples weighing between 4-8mg on a modified heat-cool-heat cycle: from 0°C to 225°C at a ramp rate of 5°C/minute, held isothermal at 225°C for ten minutes, cooled back down to 0°C at a ramp rate of 10°C/minute, held isothermal at 0°C for ten minutes, then heated again to 225°C at a ramp rate of 5°C/minute. Samples were dried for at least 24 hours before running.

Sample Printing Conditions

All samples were shaped using a Creality Ender 7 printer. Samples were printed from an ambient spool with filament diameter 1.3-2.1mm. Parts were

processed at a nozzle temperature of 220°C, bed temperature of 60°C, layer thickness of 0.2mm, print speed of 30 mm/s. Prints of tensile bars were done at two Raster Angles, 90° and 180°. (For reference, the 180° infill is parallel to the force applied during the tensile test, while the 90° is perpendicular.)

Tensile Testing

Tensile tests were run using an Instron 5944 at a speed of 10mm/s. Samples were printed to an ASTM 638 Type V standard (8mm gauge length, 3.2mm thick, 3.75mm width).

Scanning Electron Microscopy (SEM) and Energy-dispersive X-ray Spectroscopy (EDS)

All samples were dried at 110°C for 24 hours before use. The filament was cryo-fractured and placed on aluminum stubs with carbon tape. Powders were mixed by hand and placed on carbon tape. The samples were then sputter-coated with 10 nm thick Iridium. The morphology of the cross-section of the samples was observed by a JOEL IT-500HR SEM machine equipped with EDS. EDS was set to detect the elements of sodium, carbon, and magnesium.

Results and Discussion

Degradation Regimes of Raw Materials

For the composite system to be suitable for SDS, the PLA resin must degrade at a temperature well before the bentonite and zeolite. Figure 3 demonstrates that PLA degrades below 400°C, while there is no significant degradation of either clay until approximately 500°C. (The initial weight loss before 200°C is attributed to water that was still adsorbed to the clay powders even after drying.) Additionally, while some component(s) of bentonite degrade/evolve off between 500-750°C, zeolite experiences no such decomposition. Given that only one of the target clays experiences weight loss over the specified range of 500-750°C, we are able to determine the ratio of bentonite to zeolite, and therefore back out their respective compositions in a filament with PLA.

Equation 1 is used to determine the weight fraction of bentonite that degrades over the target temperature,

$$W_d = \frac{W_{500} - W_{750}}{W_{500}} \qquad \text{(Eq.1)}$$

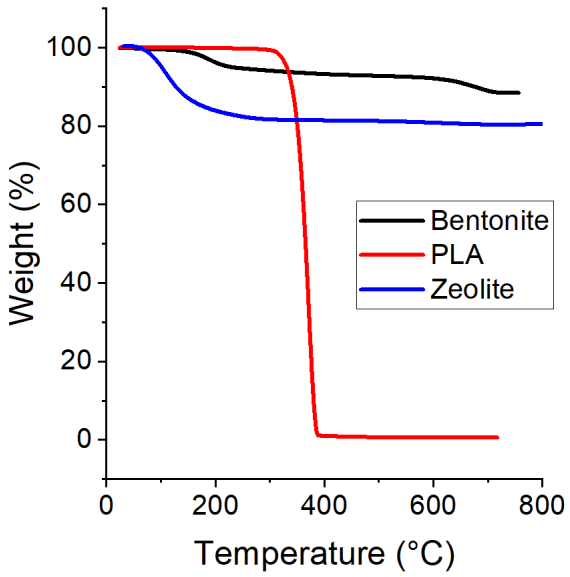

Figure 3. TGA degradation profiles of the raw material components with respect to temperature.

where W_d is the fraction of bentonite that degrades, W_{500} is the total weight fraction of material at 500°C (after PLA has degraded), and W_{750} is the total weight fraction at 750°C (after a component of bentonite has degraded). W_b is 0.048 ± 0.04 for our bentonite, meaning that there is a large enough change to be detectable in

filaments with a high enough loading percentage of bentonite. From a component mass balance, we can then determine the mass fractions of bentonite and zeolite in a composite system according to Equations 2 and 3,

$$W_b = \frac{W_{500} - W_{750}}{W_d} \qquad \text{(Eq.2)}$$

$$W_z = W_{500} - W_b \qquad \text{(Eq. 3)}$$

where W_b is the total weight fraction of bentonite in the composite and W_z is the total weight fraction of zeolite in the composite.

Filament Compounding and Importance of Adsorbed Water during Processing

Filament PBZT was compounded in a single pass via twin screw extrusion with a relatively narrow diameter distribution of 1.3-2.0 mm (Figure 4a). Filaments processed in one pass on the single screw extruder including PBZ1X_A (collected approximately 10 minutes into extrusion) and PBZ1X_B (collected as the last material from the extrusion) exhibited much broader filament

diameters (0.7-3.0 mm). A bubbling/foaming phenomenon at the nozzle of the single screw extruder suggested water vapor was evolving off, meaning the material was not sufficiently dried (Figure 4b). This bubbling made the filament difficult to draw consistently, leading to few continuous sections of filament.

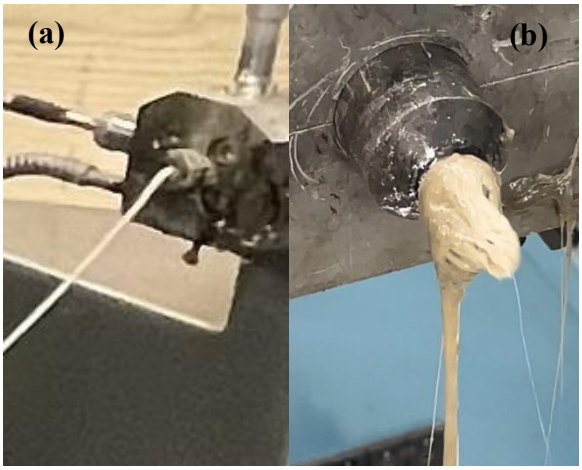

Figure 4. Filament drawing from the twin screw extruder procedure (a) and the single screw procedure (b). Bubbling and considerable die swell are visible on the single screw.

Additionally, large granules in PBZ1X_A and especially PBZ1X_B would cause clogs in the printer nozzle, meaning they were not usable for printing (Figure 5). Pelletizing the filament from the single screw and extruding again resulted in a filament (PBZ2X) with a slightly narrower diameter range (1.0mm-2.7mm), but that still exhibited similar granule formations. Therefore, no printable filament was produced through the single screw extrusion procedure.

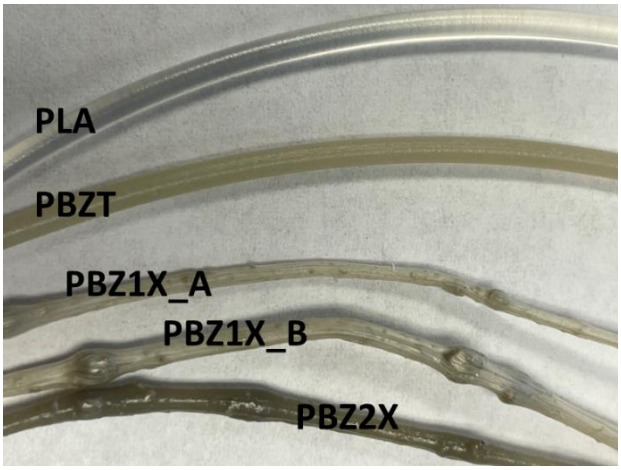

Figure 5. Compounded filaments of neat PLA, PBZT, PBZ1X_A, PBZ1X_B, and PBZ2X.

The single screw extrusion was likely unsuccessful due to the blending and interactions of the components compared to the twin screw procedure. For example, since the clays were added separately in the twin screw procedure, water vapor was able to escape before the die, unlike in the single screw. Additionally, the counter-rotating screws in the twin screw extruder may have provided a high enough shear to overcome the clays' attractive forces and prevent agglomerates from forming, while the single screw was unable to do so.

Clay Loading Levels of Compounded Filaments

Further TGA analysis was performed to estimate the true clay loading level in the compounded filaments (Figure 6). Table 1 presents the bentonite and zeolite loading levels calculated from Equations 2 and 3.

Table 1. Zeolite and bentonite percent loading (by weight) in compounded filaments.

Sample	Zeolite Loading (wt.%)	Bentonite Loading (wt.%)
PBZ2X	8.4±0.4	8.8±0.3
PBZ1X_A	5.6±0.7	6.4±0.5
PBZ1X_B	10.0±3.2	14.2±2.6
PBZT	4.9±0.7	5.8±0.7

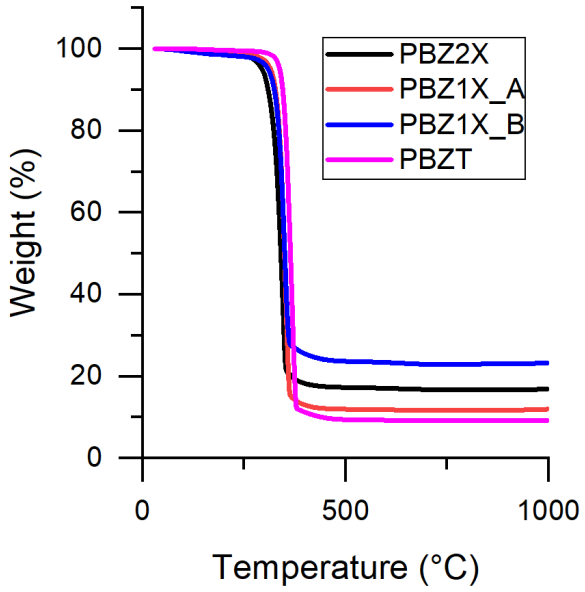

Figure 6. TGA of compounded filaments. The apparent plateau above 500°C represents the total clay loading.

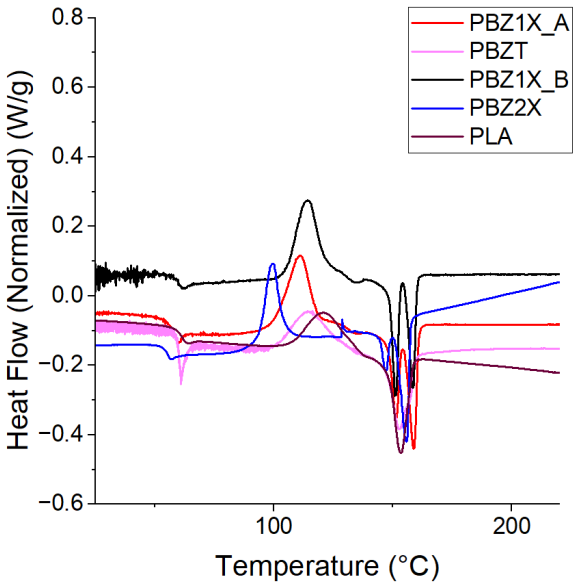

Figure 7. DSC (exotherm up) of compounded filaments. The glass transition of PLA is around 60°C and the melting temperature is approximately 160°C.

The filament from the twin screw extruder reached a loading level of approximately 10 wt.% clay, or about half the target composition. This difference is attributed to error for determining the flowrate of clays through the hopper. Despite originating from the same compounding batch, PBZ1X_A (11 wt.% clay) and PBZ1X_B (23 wt.% clay) exhibit significantly different loading levels. We attribute this to limitations from mixing and loading through one hopper, as the clay powder not adhered to PLA particles would settle and pass through the extruder last, which is why filler concentration increased over the course of the extrusion. When these filaments from single screw extrusion were pelletized and reprocessed, a filament with a more consistent clay loading of approximately 17 wt.% clay throughout was produced, much closer to the target of 20 wt.% zeolite and bentonite.

Comparison of Glass Transition and Melting Point Temperatures

DSC was performed on filaments to determine the appropriate printing conditions (Figure 7). For successful shaping via fused filament fabrication, the PLA resin of our material needs to be in the melt phase.

Filaments followed similar heat flow curves to that of the neat PLA, with a glass transition at around 60°C and a melting temperature of approximately 160°C. This melting temperature is particularly important for printing, as since it is relatively broad (over a 15°C span), printing must take place at a temperature above to ensure chains are able to flow (especially with the fillers). While secondary extrusion can assist with dispersing the clays, it comes with the drawback of added degradation of the binder. For example, PBZ2X experienced a drop in glass transitions temperature of 4.2±0.5°C compared to PBZ1X_A and PBZ1x_B, which is indicative of decreasing molecular number weight (Mn). This decrease in PLA chain length, a result of chain scission due to prolonged shear, would negatively affect the performance of our printed parts since lower molecular weight polymers have lower mechanical moduli.

Clay Dispersion and Exfoliation

The only printable filament (PBZT) was analyzed through mechanical testing for the level of clay exfoliation. Well exfoliated samples would be expected to correlate to an increase in mechanical properties, such as elastic modulus and yield strength. Figures 8 and 9 demonstrate that, for both printed infill directions, the clay filled filament did not exhibit greater mechanical properties.

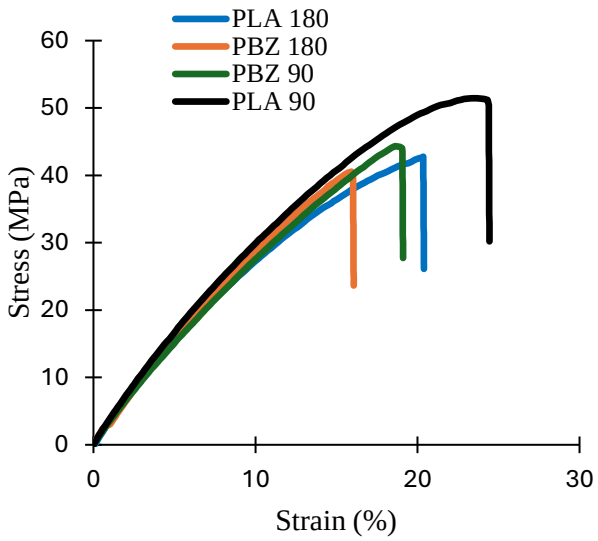

Figure 8. Tensile testing of printed samples. Those printed in a 90° infill direction (for both materials) resulted in a higher yield point.

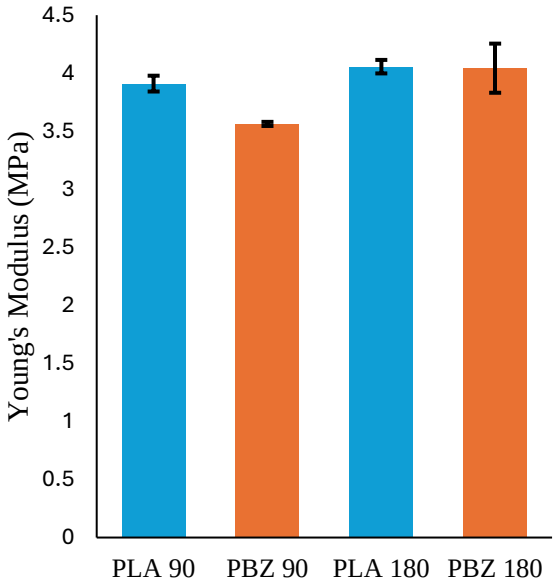

Figure 9. Young's Modulus comparisons for printed samples in both infill directions. The filled samples did not exhibit higher modulus as would be expected of well dispersed fillers.

From the mechanical testing, we realize that our clay filled parts did not experience the enhanced mechanical properties associated with bentonite exfoliation, and in fact, agglomerates are likely acting as stress concentrators, weaking the system.

Imaging of filament cross sections through SEM and EDS was performed to analyze the presence of platelets and agglomerates compared to the raw clay powders. From imaging of the neat zeolite and bentonite powders, it was confirmed that individual zeolite particles (on the scale of 1-3 µm) were much smaller than the bentonite platelet agglomerates (on the scale of 25-40 µm) (Figure 10).

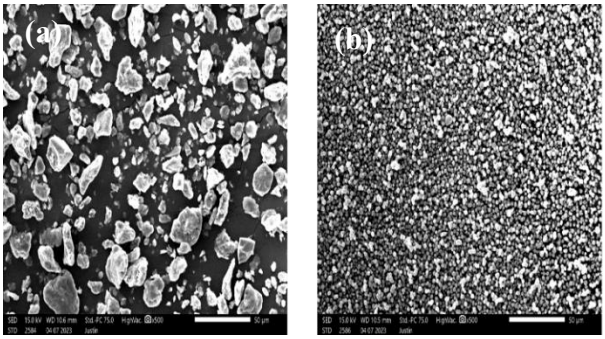

Figure 10. SEM of bentonite powder (a) and zeolite powder (b).

Additionally, it was determined that, although the atomic makeup of the clays is similar, zeolite contains significant amounts magnesium (lacking in bentonite), while bentonite contains considerable amounts of sodium (lacking in zeolite). Thus, elemental analysis allows us to differentiate among the clays in the PBZT filament cross section in Figure 11. When overlaying the magnesium elemental analysis in Figure 11b with the cross section in Figure 11a, it is observed that zeolite maintain a similar size scale (1-3µm spherical particles) to their powder form. The same process with Figure 11c for sodium demonstrated a decrease in size of the bentonite platelet agglomerates by a factor of roughly one half (10-15µm) compared to their powder form, but the platelets still maintained their greater aspect ratio compared to the zeolite particles.

This imaging corroborates the results of the tensile testing, as even though bentonite aggregates decreased in size (compared to Figure 10a), there is still a noticeable agglomeration of bentonite. The concentrated patches of sodium in Figure 11c demonstrate that the bentonite is poorly exfoliated compared to the better dispersed magnesium (zeolite) in Figure 11b.

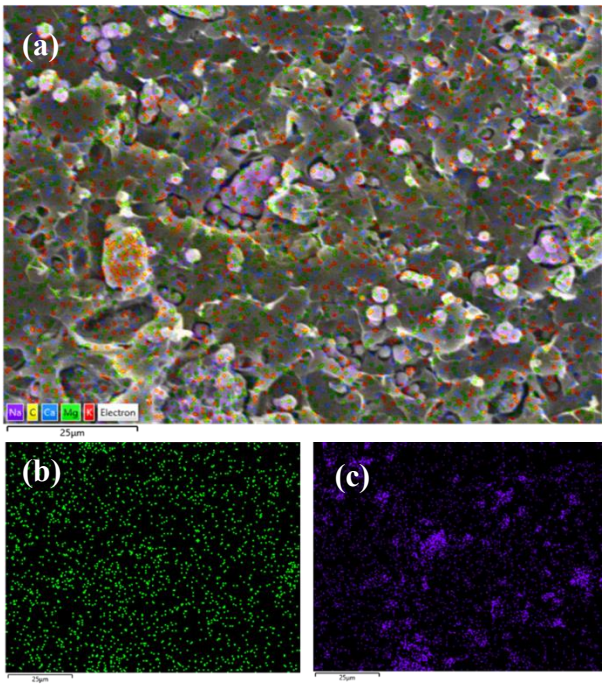

Figure 11. EDS of PBZT filament (a) with magnesium (b), corresponding to zeolite, and sodium (c), corresponding to bentonite, highlighted in the cross section.

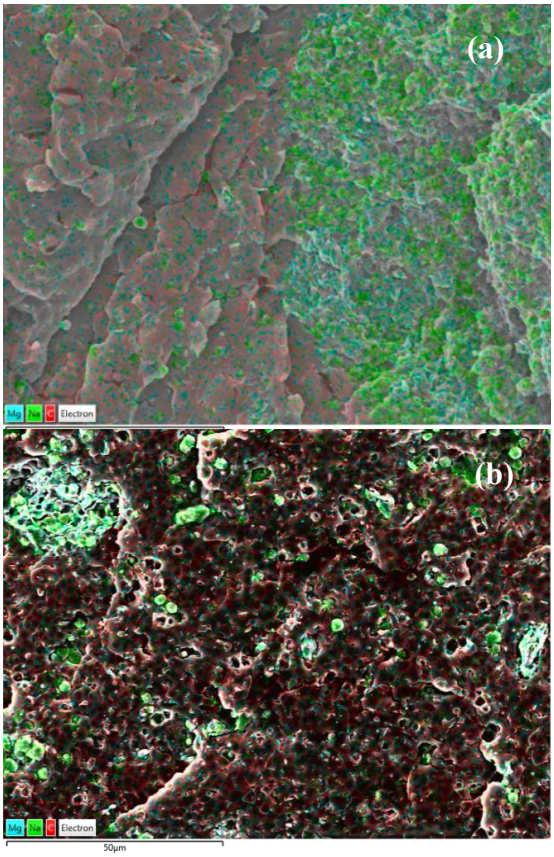

Figure 12. EDS of PBZ1X_A (a) and PBZ2X (b) filament cross sections.

Importance of Attractive Forces during Compounding

To understand the microstructural differences between the printable PBZT and unprintable filaments produced from single screw extrusion, further microscopy was performed on PBZ1X_A and PBZ2X (Figure 12). In PBZZ1X_A, the clays are poorly dispersed (concentrated on the right side of Figure 12a). Additionally, the bentonite agglomerates (15-25µm) are larger than those observed in PBZT. While both are clays are more dispersed after a second extrusion, bentonite aggregates are still more frequent and larger (15-20µm) compared to those observed in PBZT (Figure 11a). This suggests that while continuing to shear the bentonite might help with distribution throughout the filament, single screw extrusion conditions will fail to further exfoliate bentonite platelets. Similar to PBZT, zeolite particles in both PBZ1X_A and PBZ2X maintain their 1-3µm scale.

Agglomeration of the particles is likely a function of the drying conditions and inability to diffuse into the partially melted polymer. The sample Lennard-Jones potential in Figure 13 illustrates the hypothesized interparticle distances during the two extrusion conditions and the resulting intermolecular forces. As interparticle distance decreases (i.e. when water is evaporated from the interstitial space between the bentonite layers) attractive forces dominate and permanent aggregates are formed.[15] For successful extrusion using the single screw setup (preventing bubbling at the die such as in Figure 4b), intense drying of the clays was required. This included removing the water adsorbed in the zeolite, but we hypothesize this came at the cost of also removing water in the spaces between bentonite platelets. For example, feeding the polymer and clays through a single hopper in single screw extrusion could have prevented intercalation and created clay rich zones that were compacted as the polymer pellets compacted and expanded. In comparison, the twin screw added the clay particles (with some residual interstitial water from less intense drying conditions) into a fully melted polymer stream, allowing for

improved dispersion and intercalation, which was further aided by increased shear between the screws.

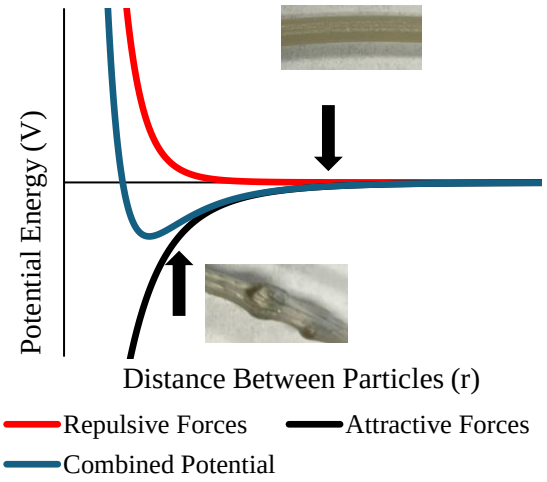

Figure 13. Lennard-Jones plot of potential energy as a function of distance between particles. Assuming that the primary intermolecular forces acting on the clay particles are electrostatic (repulsive and Van der Waal's attractive) forces, Derjaguin, Landau, Verwey and Overbeek (DLVO) theory can be used to predict the aggregation state of the particles.

Conclusions

We were able to compound novel clay filaments through two extrusion techniques and analyze their resulting properties. Filaments compounded via single screw were not printable, though a second extrusion of the same material demonstrated improvements towards the goal of printing for fused filament fabrication. Filament compounded via twin screw extrusion resulted in a printable filament. Thermal and microscopy characterizations were used to analyze the filament properties. However, both the clay loading and exfoliation of bentonite fell short of the goal for successful SDS. A higher loading percentage and better exfoliation of clay particles is required for filament that can be processed into a sintered monolith with unique geometry for air-based contaminant capture.

Author Information

*VSGC Undergraduate Research Scholar recipient

**Author to whom correspondence should be addressed (mbortner@vt.edu)

Acknowledgements

Funding for the work provided by the Virginia Space Grant Consortium. We also wish to thank Kennedy, Al; Yao, Yimin; Reynolds, John; Ballentine, Mark; Engineer Research and Development Center (ERDC), Macromolecules Innovation Institute at Virginia Tech, Virginia Polytechnic Institute and State University.

References

(1) Schunk, R. G.; Peters, W. T.; Thomas, J. T. Four Bed Molecular Sieve - Exploration (4BMS-X) Virtual Heater Design and Optimization; Charleston, SC, 2017.

(2) Knox, J. C.; Campbell, M.; Miller, L. A.; Mulloth, L. M.; Varghese, M.; Luna, B., "Integrated Test and Evaluation of a 4-Bed Molecular Sieve, Temperature Swing Adsorption Compressor, and Sabatier Engineering Development Unit". In International Conference on Environmental Systems, SAE: Norfolk, 2006, 2006-01-2271.

(3) Wise, W. S. MINERALS | Zeolites. In Reference Module in Earth Systems and Environmental Sciences; Elsevier, 2013. https://doi.org/10.1016/B978-0-12-409548-9.02906-7.

(4) Hasan, F. A.; Xiao, P.; Singh, R. K.; Webley, P. A. Zeolite Monoliths with Hierarchical Designed Pore Network Structure: Synthesis and Performance. Chemical Engineering Journal 2013, 223, 48–58. https://doi.org/10.1016/j.cej.2013.02.100.

(5) Thakkar, H.; Eastman, S.; Hajari, A.; Rownaghi, A. A.; Knox, J. C.; Rezaei, F. 3D-Printed Zeolite Monoliths for CO2 Removal from Enclosed Environments. ACS Appl. Mater. Interfaces 2016, 8 (41), 27753–27761. https://doi.org/10.1021/acsami.6b09647.

(6) Chen, M.; Liu, B.; Li, L.; Cao, L.; Huang, Y.; Wang, S.; Zhao, P.; Lu, L.; Cheng, X. Rheological Parameters, Thixotropy and Creep of 3D-Printed Calcium Sulfoaluminate Cement Composites Modified by Bentonite. Composites Part B: Engineering 2020, 186, 107821. https://doi.org/10.1016/j.compositesb.2020.107821.

(7) Bendahou, D.; Bendahou, A.; Grohens, Y.; Kaddami, H. New Nanocomposite Design from Zeolite and Poly(Lactic Acid). Industrial Crops and Products 2015, 72, 107–118. https://doi.org/10.1016/j.indcrop.2014.12.055.

(8) Thakkar, H.; Lawson, S.; Rownaghi, A. A.; Rezaei, F. Development of 3D-Printed Polymer-Zeolite Composite Monoliths for Gas Separation. Chemical Engineering Journal 2018, 348, 109–116. https://doi.org/10.1016/j.cej.2018.04.178.

(9) Lawson, S.; Newport, K.; Al-Naddaf, Q.; Ameh, A. E.; Rownaghi, A. A.; Petrik, L. F.; Rezaei, F. Binderless Zeolite Monoliths Production with Sacrificial Biopolymers. Chemical Engineering Journal 2021, 407, 128011. https://doi.org/10.1016/j.cej.2020.128011.

(10) Raj, S. A.; Muthukumaran, E.; Jayakrishna, K. A Case Study of 3D Printed PLA and Its Mechanical Properties. Materials Today: Proceedings 2018, 5 (5, Part 2), 11219–11226. https://doi.org/10.1016/j.matpr.2018.01.146.

(11) Kennedy, A. J.; Ballentine, M. L.; May, L. R.; Das, A.; Bednar, A. J.; Griggs, C. S.; Hull, M. S.; Bortner, M. J. Simplifying Complex Contaminant Mixtures: Selective Ammonia Adsorption and Toxicity Reduction Using 3D Printable Polymer–Zeolite. Water Air Soil Pollut 2022, 233 (5), 148. https://doi.org/10.1007/s11270-022-05606-9

(12) Gonzalez-Gutierrez, J.; Cano, S.; Schuschnigg, S.; Kukla, C.; Sapkota, J.; Holzer, C. Additive Manufacturing of Metallic and Ceramic Components by the Material Extrusion of Highly-Filled Polymers: A Review and Future Perspectives. Materials 2018, 11 (5), 840. https://doi.org/10.3390/ma11050840.

(13) Zhu, T. T.; Zhou, C. H.; Kabwe, F. B.; Wu, Q. Q.; Li, C. S.; Zhang, J. R. Exfoliation of Montmorillonite and Related Properties of Clay/Polymer Nanocomposites. Applied Clay Science 2019, 169, 48–66. https://doi.org/10.1016/j.clay.2018.12.006.

(14) de las Heras, D.; Schmidt, M. Bulk Fluid Phase Behaviour of Colloidal Platelet–Sphere and Platelet–Polymer Mixtures. Phil. Trans. R. Soc. A. 2013, 371 (1988), 20120259. https://doi.org/10.1098/rsta.2012.0259.

(15) Liu, L.; Moreno, L.; Neretnieks, I. A Dynamic Force Balance Model for Colloidal Expansion and Its DLVO-Based Application. Langmuir 2009, 25 (2), 679–687. https://doi.org/10.1021/la8026573.